UCRL-15918
I/O 6201605/NM

Compact Torus Studies
Final Report

Edward C. Morse

June 1987

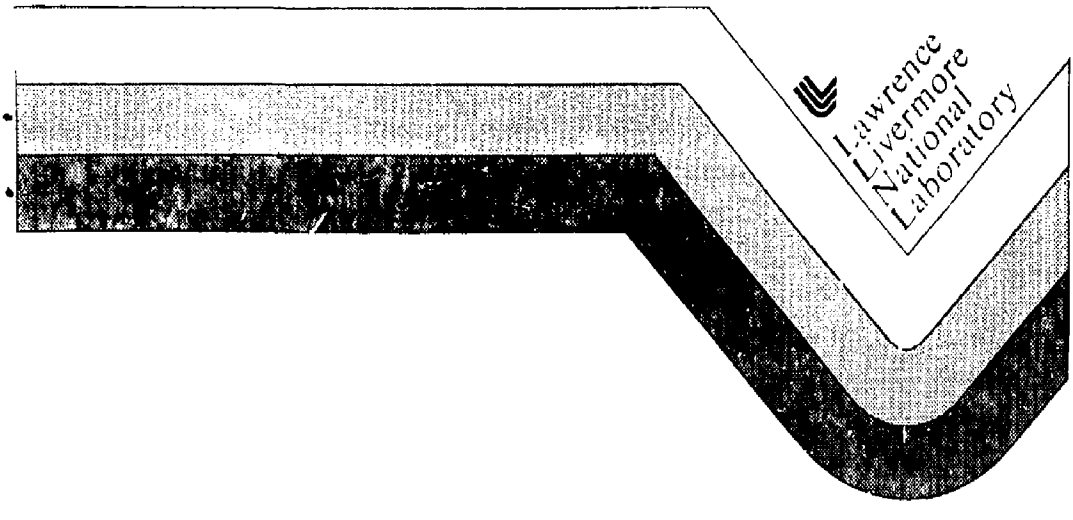

DISCLAIMER

Work performed under the auspices of the U.S. Department of Energy by Lawrence Livermore National Laboratory under contract number W-7405-ENG-48.

UCRL-15918
I/O 6201605

UCRL--15918

DE87 014254

COMPACT TORUS STUDIES

Final Report

Submitted to Lawrence Livermore Laboratory

Technical Contact: Richard Ziolkowski

In partial fulfillment of contract

Principal Investigator: Edward C. Morse

College of Engineering
Office of Research Services
University of California
Berkeley, CA 94720

0. Introduction and Overview

The following report describes the activities carried out at Berkeley under contract with Lawrence Livermore Laboratory in the area of compact torus applications studies.

The compact torus (CT) device has been proposed for use in some applications which are of interest in Laboratory programs in the areas of pulsed power and inertial confinement fusion. These applications involve compression and acceleration of CT plasmas. The RACE (Ring Accelerator Experiment) experimental program at Livermore has been initiated to study these applications.

The work reported here involves studies of plasma physics and other aspects of these compact torus applications. The studies conducted identify specific problem areas associated with the CT device and examine these areas in some detail.

This report contains studies of three particular problem areas of the CT applications. These three areas are: (1) the general nonlinear properties of the CT as a magnetohydrodynamic (MHD) equilibrium, (2) particle simulation of the compression of the CT, with a focus on the non-MHD effects, and (3) nonlinear RF interaction problems in the CT.

This report is organized into three sections. Each section contains the most important results in each of the three areas outlined above. A section of comments and conclusions follows.

1. Nonlinear Properties of Compact Toroids

The most interesting aspect of existing CT plasma experiments is the observed longevity of the CT plasmas. The plasmas are known to exist for periods which are long compared to Alfven times, which is indicative of absence or suppression of MHD instability (Ref. 1). CT plasmas have also shown stability to translation through a magnetized cylinder, as was demonstrated in the FRX-C experiment at Los Alamos.

Two aspects of the physics of the CT device that support the experimental observations should be mentioned here. First, the CT plasma state represents a Taylor minimum state. This means that the CT plasma configuration is one which has minimum magnetic energy for a given value of the so-called magnetic helicity, K, which is defined as:

$$K = \int d^3x \, \vec{A}\cdot\vec{B} \qquad (1)$$

Here A is the vector potential, defined so that $\vec{B} = \nabla\times\vec{A}$. The minimization of the magnetic energy $W = \int d^3x B^2/2$ with constant K results in an Euler equation of the form:

$$\vec{\nabla}\times\vec{B} = \lambda\vec{B}$$

where λ is the helicity constant such that

$$\lambda^{-1} = \frac{\int d^3x \vec{A}\cdot\vec{B}}{\int d^3x \vec{B}\cdot\vec{B}} = \frac{K}{2W}$$

The solution to this eigenvalue problem for boundary conditions such that the magnetic poloidal flux vanishes on a sphere of radius a is given by:

$$\vec{B} = \vec{\nabla}\psi \times \vec{\nabla}\phi + a\psi\vec{\nabla}\phi \quad , \quad \psi = \psi_0 \sin^2\theta \sqrt{r/a}\, J_{\frac{3}{2}}(\lambda r)$$

Here the helicity eigenvalue λ is chosen such that λa is a root of the Bessel function, and the first nontrivial root is at $\lambda a = 4.49$.

This solution has been analyzed theoretically by Bussac and Rosenbluth (Ref. 2), who showed that internal MHD modes are not unstable in this configuration, and that only singular modes at the plasma edge are unstable. These modes are presumably stabilized by such non-MHD features as finite ion Larmor radius and by line-tying.

Another aspect of the physics of the CT device which may account for its longevity is the similarity of its structure to known vortex soliton states in plasma (Ref. 3). These states are cases where the dispersive properties of the Alfvenic medium are balanced by the nonlinear terms in the MHD equations. In Ref. 3, the authors use a special hybrid model of the plasma response that retains the dielectric terms responsible for ion-acoustic waves as well as the usual MHD flow-like terms giving Alfven wave roots. They then analyze these equations in a strictly two-dimensional coordinate system (i. e. infinite in one dimension) and find that with a simplifying assumption (with one component of the A-potential stream function negligible comapred to another) that the equation set then is an exact duplicate of the two-dimensional Rossby wave equation arising in oceanography (Ref. 4).

There are several problems in the direct comparison of the vortex soliton found in Ref. 3 and the case with the propagation of the CT. The most obvious is that the solution in Ref. 3 is a two-dimensional vortex, with a stream function expressed in terms of first-order Bessel function in radius and a term linear in radius:

$$\chi = a \sin\theta \left[AJ_1(kr) - r\left(\frac{\beta - Uk^2}{k^2}\right)\right] = \sin \qquad (2)$$

The comparison with (1) is interesting, however, in spite of the different geometry. A more significant difference is the requirement that the z-component of the vector potential is negligible compared to the perpendicular components. Secondly, the soliton of Ref. 3 must propagate obliquely to the magnetic field, and that propagation at angles small with the magnetic field requires that the perturbation is very samll. Thus the solution is evidence of solitonic states for closed plasma vortices, but does not represent the CT state very well.

In an attempt to find more general solutions in the MHD domain, we expand on the original method used by Larichev, et. al. (Ref. 4) for derivation of the Rossby soliton.

Starting with the Navier-Stokes equation in cylindrical coordinates, assuming cylindrical symmetry and no fluid velocity in the azimuthal direction ($u_\theta = 0$):

$$u^R_t + u^R u^R_R + u^Z u^R_Z = \frac{1}{\rho}\left[-P_R + J_\theta B_Z\right]$$

$$u^Z_t + u^R u^Z_R + u^Z u^Z_Z = \frac{1}{\rho}\left[-P_Z + J_\theta B_R\right] \qquad (3)$$

We now substitute the potential functions χ and ψ for the velocity stream functions and poloidal magnetic flux functions, respectively. The basic velocities and fields are then defined in terms of these potentials by:

$$\vec{u} = -\frac{\hat{R}}{R}\chi_Z + \frac{\hat{Z}}{R}\chi_R$$

$$\vec{B} = -\frac{\hat{R}}{R}\psi_Z + \frac{\hat{Z}}{R}\psi_R \qquad (4)$$

We then substitute these into the Navier-Stokes equation, first imposing the requirement that solutions carry time dependence only in the form $f(r,z,t)=f(r,z-Ut)$. The resulatnt equations are:

$$U\left(\frac{\chi_Z}{R}\right)_Z + \left(\frac{\chi_Z}{R}\right)\left(\frac{\chi_Z}{R}\right)_R - \left(\frac{\chi_R}{R}\right)\left(\frac{\chi_Z}{R}\right)_Z = -\frac{1}{\rho}\left(P_R + \frac{\psi_R \Delta^*\psi}{R^2}\right) \qquad (5)$$

$$-U\left(\frac{\chi_R}{R}\right)_Z - \left(\frac{\chi_Z}{R}\right)\left(\frac{\chi_R}{R}\right)_R + \left(\frac{\chi_R}{R}\right)\left(\frac{\chi_R}{R}\right)_Z = -\frac{1}{\rho}\left(P_Z - \frac{\psi_Z \Delta^*\psi}{R^2}\right) \qquad (6)$$

We now transform away the time-like terms by forming an effective stream function $\chi'(R,Z) = \chi(R,Z) + 1/2UR^2$. With this substitution, we now obtain the more balanced form:

$$\rho R\left[\chi', \frac{\chi_Z}{R}\right] = \psi_R \Delta^*\psi + R^2 P_R \qquad (7)$$

$$\rho R\left[\chi', \frac{\chi_R}{R}\right] = -\psi_Z \Delta^*\psi - R^2 P_Z \qquad (8)$$

Here the bracket operator [A,B] is a Lie commutator or Poisson bracket on the space R,Z, defined by:

$$[A,B] = A_R B_Z - A_Z B_R \qquad (9)$$

Differentiating Eq.(7) by Z and equation (8) by R and then adding the two equations, we arrive at the following form:

$$\left(R[\chi', \frac{\chi_Z}{R}]\right)_Z + \left(R[\chi', \frac{\chi_R}{R}]\right)_R = [\psi, \Delta^*\psi] - 2RP_Z \qquad (10)$$

We now simplify Eq. (10) by the observation of another bracket equation, namely:

$$[\frac{\psi_R'}{R}, \frac{\psi_R}{R}] = 0 \qquad (11)$$

With this substitution, we have the suprisingly simple form:

$$\rho[\chi', \Delta^*\chi] = [\psi, \Delta^*\psi] - 2RP_Z^* \qquad (12)$$

or alternatively

$$\rho[\chi', \frac{\Delta^*\chi}{R^2}] = [\psi, \frac{\Delta^*\psi}{R^2}]$$

This equation forms the basic Lie group of solutions to the nonlinear cylindrical MHD equations shown above. For example, notice how the Hill's vortex solution forms a solution for both the stream function, when no magnetic terms are present, or as a stationary MHD equilibrium, when no flow terms are present. This solution is given by:

$$\chi_\psi = bR^2(1 - R^2 - Z^2) \qquad (13)$$

Here b is a constant determined by the flow velocity at infinity for the one solution or by the magnetic field at infinity in the other. General classes of solucions are formed by finding particular forms from the bracket equations and superposing homogeneous forms from the roots of the brackets, such as:

$$\Delta^*\psi_1 = \lambda_\psi\psi_1 \quad , \quad \psi = \psi_0 + \psi_1$$

$$\Delta^*\chi_1 = \lambda_\chi\chi_1 \quad , \quad \chi = \chi_0 + \chi_1 \qquad (14)$$

We note the interesting result that the "homogeneous" terms in the solution are the force-free Taylor solutions, for both the stream function and for the flux function. Thus the Taylor solutions in this geometry form the basis for the transformation of a solution to the coupled equations into another solution using the Lie method.

All allowed solutions of this type must also solve the magnetic diffusion equation, which can also be written in Lie form by the commutator relation:

$$[\chi, \psi] = \beta R \tag{15}$$

Solutions admitted by this bracket equation have the form:

$$\psi = \alpha\chi + \gamma R^2 \tag{16}$$

We can now form self-consistent flow equilibria by solving the coupled set of bracket equations. Equally importantly, we can identify the transformation properties of the solutions through the identification of the Lie brackets involved.

At the time of this report, a thorough study of the solitonlike solutions to equations (13) and (15) of relevance to the moving compact toroid problem has not been undertaken. However, the mathematical technique outline here certainly will aid in the development of a full mathematical model of the motion of solitonlike, 3-dimensional vortex states.

2. Particle Simulation of Compact Toroid Compression

We now turn our attention to the computer simulation studies carried out in this contract period of relevance to the CT compression studies. This work was carried out by the principal investigator with the assistance of a graduate student, Scott Parker.

In order to simulate the compression of the CT plasma in the conical flux conserver of the RACE experiment using conventional electromagnetic particle simulation, a simplified dynamical analog to the problem was posed. This analogous problem is to assume that the CT plasma is at rest and that the walls were being moved in against the plasma radially. In this way, problems with moving meshes were avoided, and boundary conditions were kept in the quasi-static electromagnetic domain.

The particle simulation code used to carry out these studies is the RINGHYBRID code developed by A. Freidman (Ref. 5). In this code, axisymmetric self-consistent plasma states can be studied using ion particle kinetics in the Darwin limit, i. e. elctrostatic effects are ignored, and ion currents contribute to the poloidal magnetic field. In this code, only poloidal (R,Z) magnetic field terms are kept, and only toroidal ion currents are collected. The code can run dynamically, that is, with a continual collection of ion currents, and with induction electric fields present allowing for the change in B. Although the code also contains a first-order linearized mover, with linearized field solves in azimuthal Fourier components, the first order package was not used. This package can be used to analyze the MHD stability of the plasma equilibria, which makes no sense to operate when the plasma is dynamically evolving on a fast rate compared to the Alfven transit time.

The basic equations solved in this code are the ion equations of motion:

$$\frac{d\vec{v}_j^i}{dt} = \frac{q}{m}\left[\vec{E}(\vec{x}_j) + \frac{\vec{v}_j^i}{c} \times \vec{B}(\vec{x}_j)\right] \qquad (17)$$

as well as the Maxwell equations:

$$E_\theta = -\frac{1}{c}\dot{A}_\theta \qquad (18)$$

$$\vec{B}_{pol} = \vec{\nabla} \times \vec{A}_\theta \qquad (19)$$

$$\left(\nabla^2 - \frac{1}{R^2}\right) A_\theta = -\frac{4\pi}{c^2} \sum_j q_j v_{i\theta}^j \delta(x-x^j) \qquad (20)$$

The particle positions and velocities are advanced by a leapfrog technique, using a second-order accurate Boris integrator. The field equations are developed from the particle velocity and position data using a predictor-corrector technique. The algorithm is vectorized only in the outer loops, and the block structuring is not as elegant as some newer codes. As a result, the runs take typically twenty minutes of C-machine time for 1000 timesteps.

The compression was simulated by modifying Freidman's original algorithm by the inclusion of movable boundary conditions in the fieldsolve package. The A-theta laplacian inversion routine is done using a successive over-relaxation technique in subroutine SOR9. Here the boundary condition at the wall (E-tan=0) was enforced by setting the vector potential in the cell just outside the wall equal to the inverse of the A-potential in the cell just inside the wall. In this way, matrix inversion could be effected in a nonsingular way. By changing the cell at which this calculation is done, the boundary can be caused to effectively move. In order to retain Gallilean invariance, however, the new boundary condition must be set as

$$\vec{E} + \vec{v} \times \vec{B} = 0,$$

where v is the velocity of the wall. However, in the parameter range of interest in this problem, the difference between this boundary condition and the simpler one E-tan=0 is negligible, and the simpler boundary condition was used in the code.

A more important restriction in the accuracy of the simulation is the requirement of resistivity in the algorithm. If the resistive term in the Maxwell equation above is turned off, anomalously large electric fields will be generated in the code. This is due to the predictor-corrector algorithm, which is not stable against high-frequency perturbations in the ion current. If the wall motion generates high-frequency pulses or current spikes, the predictor-corrector algorithm may not converge correctly, and the result is a massive dump of particles and field energy. The inclusion of a small amount of resistivity can overcome this problem, since it tends to make the dielectric constant resistive on a short timescale, while retaining the

overcome this problem, since it tends to make the dielectric constant resistive on a short timescale, while retaining the basic magnetoinductive character of the dynamics on the longer timescale.

With these caveats, the sample results of the simulation for two different compression rates are shown here as Figs. 1 through 17. From these simulations, one can notice some qualitative features tnhat differ from the previous MHD simulations by Eddleman (Ref. 6). In both cases, the compression of the plasma caused it to lengthen. The five-to-one compression in wall radius caused a three-to-one increase in the aspect ratio. In the MHD studies, the compressions were nearly self-similar, and the aspect ratio stayed relatively constant. We interpret this to be caused by some non-adiabatic effects in the compressions applied here. For the two cases here, $\mu_i \hat{c}$ =1.5 and $\omega_c \hat{c}$ =7.8. While this may seem long enough to retain good conservation of the magnetic moment invariant, it is probably sufficient to destroy the bounce-averaged flux invariant, since the compression time is short compared to ion bounce times. It remains to be seen, however, if the other components of the magnetic field would change this, since in general the RACE compact toroids carry some toroidal fields as well. This invites the possibility that poloidal electric fields would be present. However, a high-beta MHD equilibrium such as Hill's vortex also shows self-similarity during compression, and that is the MHD fluid analog of the particle equilibrium used in our RINGHYBRID simulations. Thus the self-similarity seen in Eddleman's runs may be due to their MHD-like properties rather than their inclusion of toroidal field.

As another observation on the two simulation runs shown here, note that the faster of the two compression runs shows some signs of doublet formation. The particle density clearly peaks off the midplane in this run. There is some evidence of two separate O-points at the two density peaks in the poloidal plane.

This is a behavior that is not allowed in ideal MHD, as it implies a magnetic reconnection. It is perhaps significant that this process only happens in the faster compresssion, for this run contains dynamical frequencies well above the Alfven time. Since the particle simulation codes of this type have shown topological changes of a type seen only in resistive MHD, they frequently carry similar physics. In the particle simulation, the virtually infinite degrees of freedom accompanying the coupled set of ion equations of motion and Maxwell's equations can break the symmetry of MHD in a way resembling resistive MHD. Thus the reconnection process here proceeds in a way similar to the classic Kadomstev reconnection process that is frequently employed im resistive MHD theory.

On a practical note, the occurence of doublet formation in the accelerated compact torus studies could be very detrimental. Since the presence of two O-points implies that fieldlines at the radius of the null but on the midplane now connect to flux surfaces on the outside of the null, particle energy now has a

shorter trip to make before it is transported to the wall. Thus doublet formation is likely to be accompanied by increased energy loss to the wall. This in turn implies that resistive losses will be higher, and thus the effective L/R time is shortened. Thus experimentally, doublet formation would appear as anomalously fast ring decay. This may place an upper bound on the compression rate, and thus the velocity at which the CT plasma enters the conical flux conserver.

3. Nonlinear RF Properties of Compact Toroids

In one of the applications of the compact torus planned in the RACE experiment, the CT is to be used as a moving piston to pulse the RF energy out of a microwave resonant cavity charged with large amplitude RF fields. In this scheme, the CT is expected to move into the cavity with a velocity on the order of 0.1c. The resulatnt J-conservation of the photon continuum in the cavity will cause the RF frequency to be upshifted, and the stored energy increased. As the frequency is raised a coupling waveguide becomes p.opagative rather than evanescent, and the cavity's RF energy is quickly transferred into the waveguide. In this manner, kilojoules of stored RF energy can hopefully be pulsed in a few oscillation periods, which results in power levels in the hundreds of gigawatts.

It is crucial in this scheme that the CT plasma remains relatively impenetrable to the RF energy stored in the cavity. The linear coupling relations determine that the CT plasma will not couple well to the RF if there is an unmagnetized sheath in front of the equilibrium with a sufficiently high density to provide a plsama-frequency cutoff. However, some tunnelling may occur, due to the finite sheath thickness, and it remains to be seen whether the CT device is absorptive to the leakage RF fields.

For the parameters of the experiment, with densities on the order of 1.0 E 23 per cubic meter, and temperatures on the order of 100 eV, with magnetic fields on the order of 150 Tesla, the pump frequency chosen (10.0 GHz) falls within the device's lower hybrid resonance at some point in the interior of the CT. Thus we have commenced a study of nonlinear RF effects at the lower hybrid frequency in the CT. A linear ray tracing study of the lower hybrid wave propagation in the CT was done several years ago by the investigator (Ref. 7), and the RF waves are found to propagate to a lower hybrid resonance inside the device. The analysis did not include the absorption mechanism at resonance, which is a rather complicated process at lower hybrid resonance. However, the study did show the accessibility of the lower hybrid energy to the resonance in the CT geometry.

In the present study, we present some details of the nonlinear processes in the lower hybrid band in the CT plasma. The description of the nonlinearity is done by identifying the coupling modes for parametric decay instabilities in terms of the parent and daughter waves, and to calculate the threshold electric fields required for excitation of these parametric decays. This section of the report was done with the assistance of garduate student Iyad Dajani.

A wave in a plasma can be thought of as a time-dependent equilibrium state. If such a system is unstable, it is called parametrically unstable, the "parameter" being the amplitude of the single wave. Parametric excitation of coupled waves can be described as follows: Consider two waves with frequencies ω_1, ω_2. Consider the interaction of these two waves with a third one of frequency ω_0 such that $\omega_0 = \omega_1 + \omega_2$. Then energy can be converted from the third wave (ω_0) to the other two.

In order to analyze possible coupling schemes, we first construct Stokes diagrams , showing vs. k for the initial pum wave. These diagrams are shown as Figures 18 and 19 for the cold propagation case and the warm propagation case. In both cases, the digrams are plotted for three values of the propagation angle expressed as $\cos^2\theta$. Note that only for rather small angles relative to normal, i. e. $O(m_e/m_i)$, are the lower hybrid waves propagative.

Here we consider decay into quasi-ion modes. These are wave modes analogous to ion Bernstein waves, but they are waves that do no exist without the perturbing electric field from the pump wave. The perturbing electric field, in effect, causes the ion "temperature" required to excite the Bernstein-like waves. The waves are analyzed in the domain where $T_i < T_e$ and where $\cos^2\theta \frac{m_e}{m_i} \gtrsim 1$. The threshold condition for decay of the pump wave into quasi-ion modes in the dipole approximation has been obtained by Porkolab (Ref. 8):

$$\frac{U}{V_s} = \frac{2\omega_0}{\omega_{pi}} \left(\frac{2.6\gamma}{\omega_2} \right) \left(1 + \frac{\omega_{pe}^2}{\omega_{ce}^2} \right)^{\frac{1}{2}} \qquad (21)$$

where

$$U = \frac{E_0}{B} \quad , \quad V_s = \left(\frac{kT_e}{m_i} \right)^{\frac{1}{2}} \quad , \quad \gamma_2 = \frac{\varepsilon_{im}(\omega_2)}{\left(\frac{\partial \varepsilon_R}{\partial \varepsilon_k} \right)} \qquad (22)$$

and

$$\varepsilon_{im}(\omega_2) = \left(\frac{\omega_{pe}^2}{\omega_2^2} \cos^2\theta + \frac{\omega_{pi}^2}{\omega_{ce}^2} \sin^2\theta \right) \frac{\nu_e}{\omega_2} + \frac{\omega_{pi}^2 \nu_i}{\omega_2^2} + \frac{\sqrt{\pi}}{k^2 \lambda_D^2} \frac{\omega_2}{k_\parallel v_{th}} \exp\left(\frac{-\omega_2^2}{k_\parallel^2 v_{th}^2} \right)$$

Here $v_{the}^2 = 2T_e/m_e$ is the electron thermal velocity, and λ is the Debye length.

We now investigate the matching conditions required for coupling of the lower hybrid wave to the quasi-ion modes. Using the warm-plasma dispersion relation for lower hybrid waves as derived by Stix (Ref. 8):

$$\varepsilon N_{\perp}^{6} + AN_{\perp}^{4} + BN_{\perp}^{2} = 0 \quad , \tag{24}$$

where the coefficients A, B, and C are:

$$A = 1 + X(y - \alpha) \quad , \quad B = -\mu X N_{||}^{2}(1 - (A + XY) N_{||}^{-2}),$$

$$C = \mu^2 X^2 Y, \quad X = \omega_{pe}^2 (\mu\omega^2)^{-1}, \quad Y = \mu\omega^2(\omega_{ce})^{-2}, \tag{25}$$

$$\mu = m_i m_e^{-1} \quad , \quad \gamma = \sum \frac{n_i}{n_e} Z_i^2 A_i^{-2}$$

We can now proceed to obtain a numerical estimate for the electric field amplitude given by Porkolab's estimate for the parameters of the RACE experiment. For hydrogen ions and a propagation angle $\cos^2\theta = 1.0$ E-5, we obtain $\vec{E}_0 = 2.0$ kV/m. This results in a threshold power density of 5 megawatts per square meter. As the electric field amplitudes in the proposed RF compressor experiment are on the order of 1.0 E8 volt per meter, we see that isolation better than 100 dB between the plasma interior and the RF compression fields would be required in order to negate the effects of parametric instability.

5. References

1. W. C. Turner et. al., Phys. Fluios 26, 1965 (1983).

2. M. N. Rosenbluth and M. N. Bussac, Nucl. Fusion 19, 489 (1979).

3. A. B. Mikhailovskii, G. D. Aburdzhaniya, O. G. Onischenko, and A. P. Chirikov, Physics Letters 101A, 263 (1984).

4. V. D. Larichev and G. M. Reznik, Dokl. Akad. Nauk SSSR 231,1077 (1976)., see also D. R. Wells, Phys. Fluids 9,1010 (1966).

5. A. Friedman, Simulation Studies of the Stability of Strong Ion Rings, Ph. D. Thesis, Cornell University, 1980.

6. S. Maxon and J. Eddleman, Phys. Fluids 21, 1856 (1978).

7. E. Morse and Z. Mikic, Fusion Technology 3, 311 (1983).

8. M. Porkolab, Phys. Fluids 17,1432 (1974); also Phys. Fluids 17, 1592 (1974).

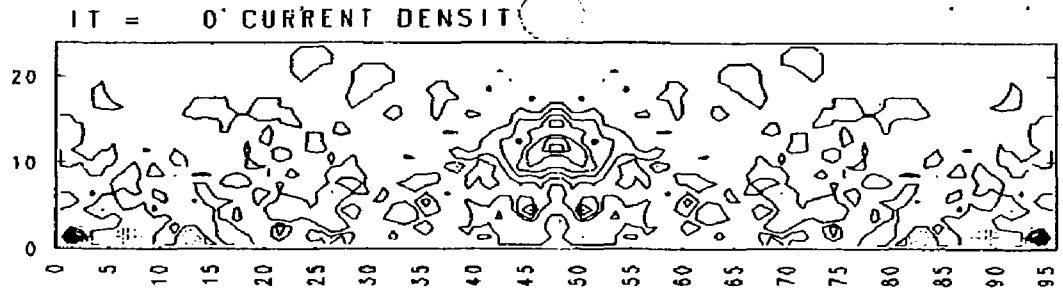
IT = 0 CURRENT DENSIT
20
10
0
0 5 10 15 20 25 30 35 40 45 50 55 60 65 70 75 80 85 90 95

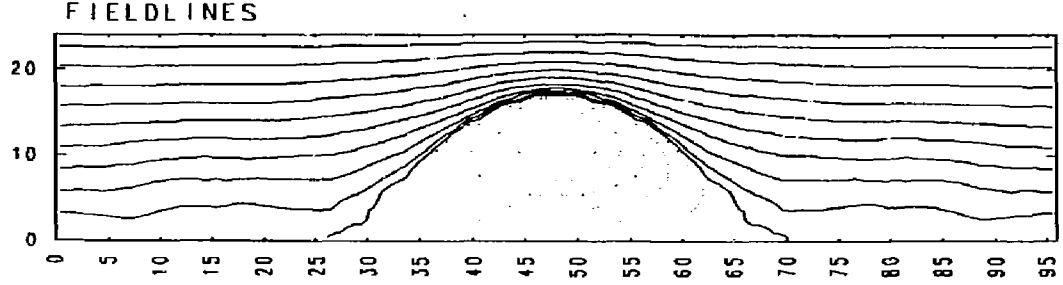
FIELDLINES
20
10
0
0 5 10 15 20 25 30 35 40 45 50 55 60 65 70 75 80 85 90 95

EXDA

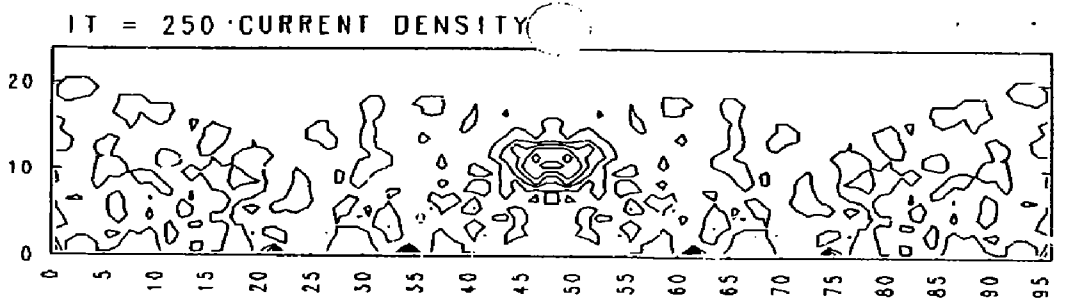
IT = 250 CURRENT DENSITY
20
10
0
0 5 10 15 20 25 30 35 40 45 50 55 60 65 70 75 80 85 90 95

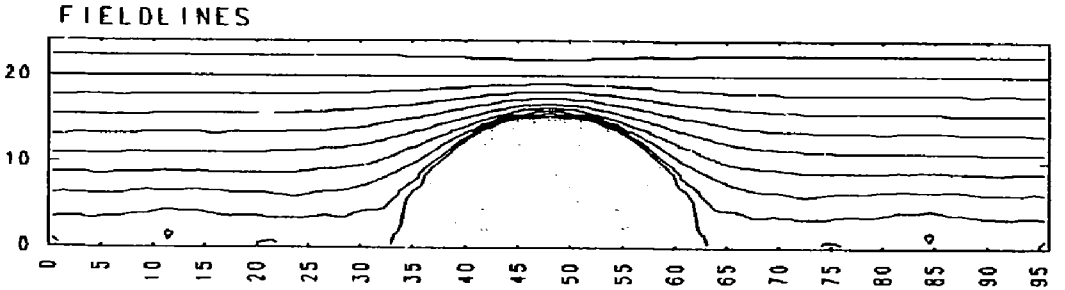
FIELDLINES
20
10
0
0 5 10 15 20 25 30 35 40 45 50 55 60 65 70 75 80 85 90 95

EXDA

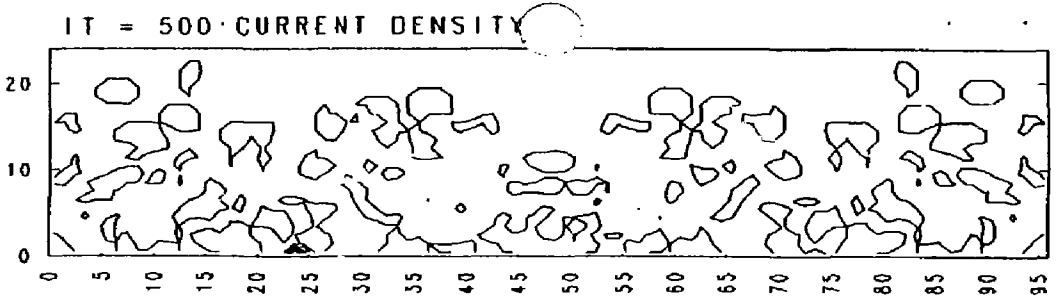
IT = 500 CURRENT DENSITY
20
10
0
0 5 10 15 20 25 30 35 40 45 50 55 60 65 70 75 80 85 90 95

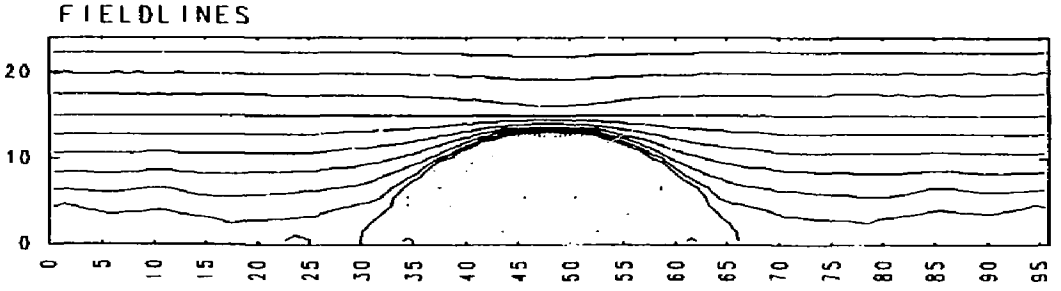
FIELDLINES
20
10
0
0 5 10 15 20 25 30 35 40 45 50 55 60 65 70 75 80 85 90 95

EXDA

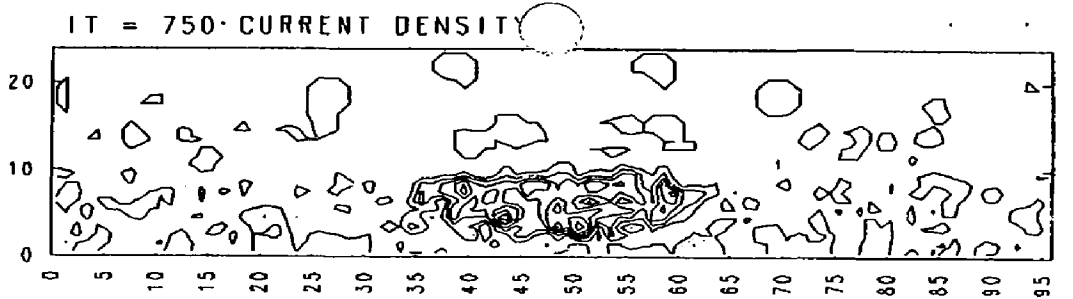
IT = 750· CURRENT DENSITY
20
10
0
0 5 10 15 20 25 30 35 40 45 50 55 60 65 70 75 80 85 90 95

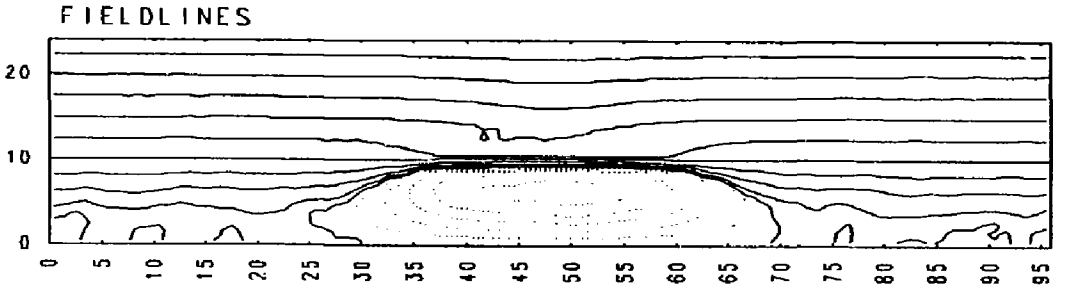
FIELDLINES
20
10
0
0 5 10 15 20 25 30 35 40 45 50 55 60 65 70 75 80 85 90 95

EXDA

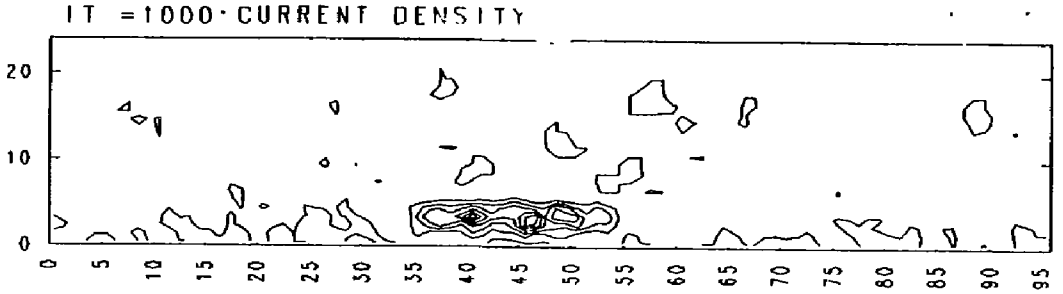
IT =1000·CURRENT DENSITY
20
10
0
0 5 10 15 20 25 30 35 40 45 50 55 60 65 70 75 80 85 90 95

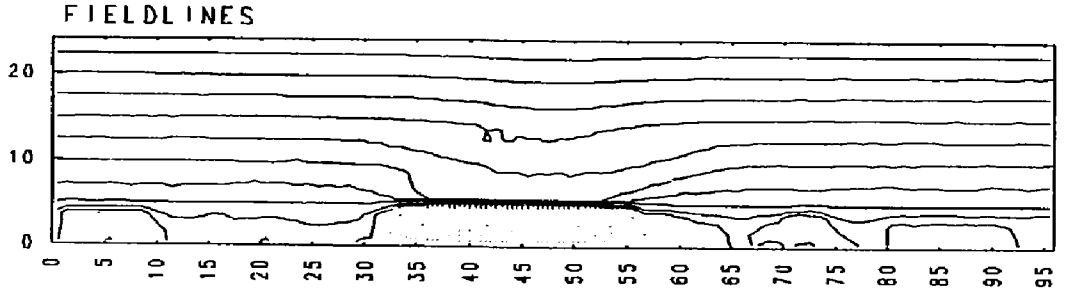
FIELDLINES
20
10
0
0 5 10 15 20 25 30 35 40 45 50 55 60 65 70 75 80 85 90 95

EXDA

NUMBER OF PARTICLES

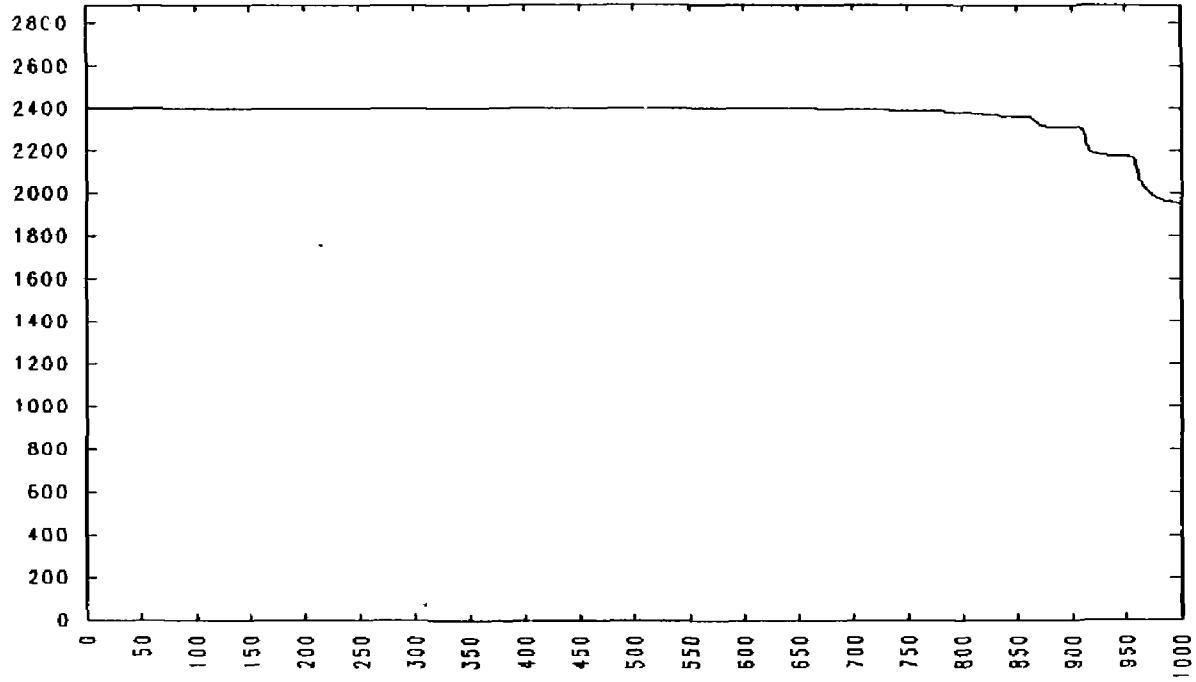

EXDA

BZX , BZMAX , BZAXIS

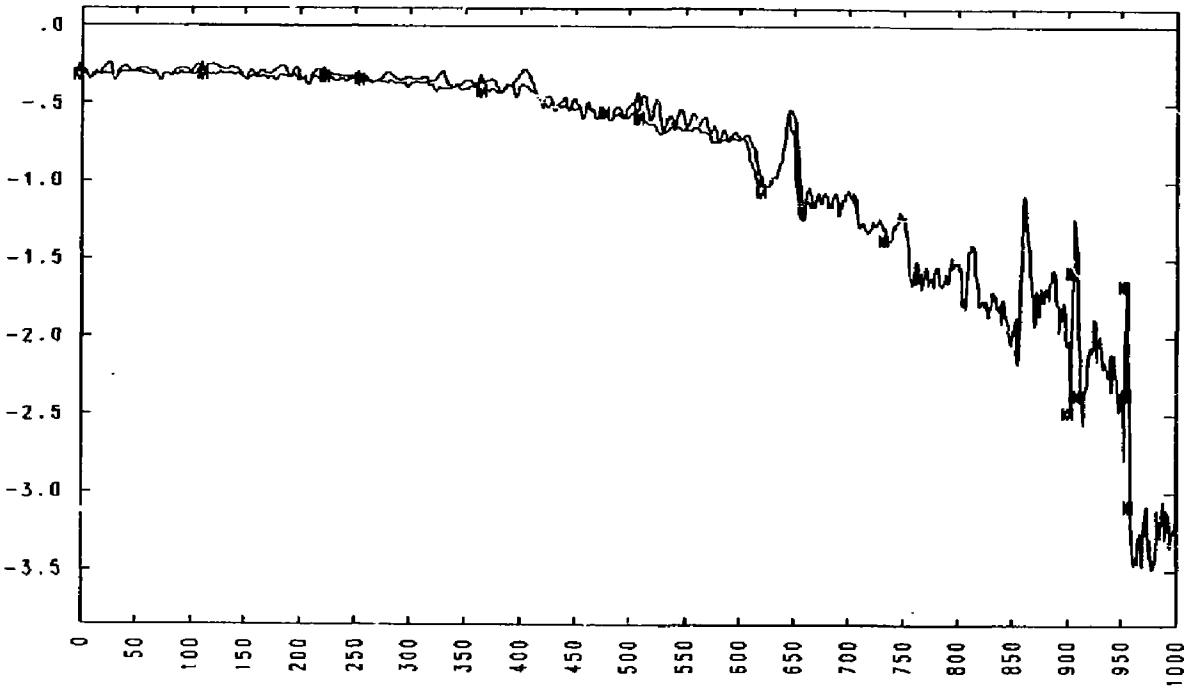

EXDA

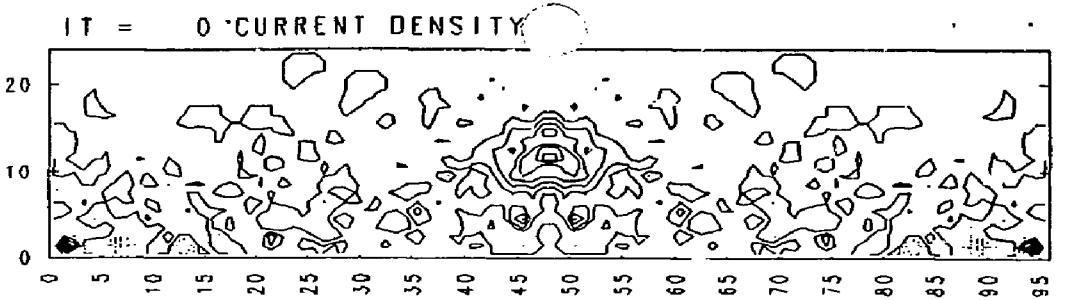
IT = 0 CURRENT DENSITY
20
10
0
0 5 10 15 20 25 30 35 40 45 50 55 60 65 70 75 80 85 90 95

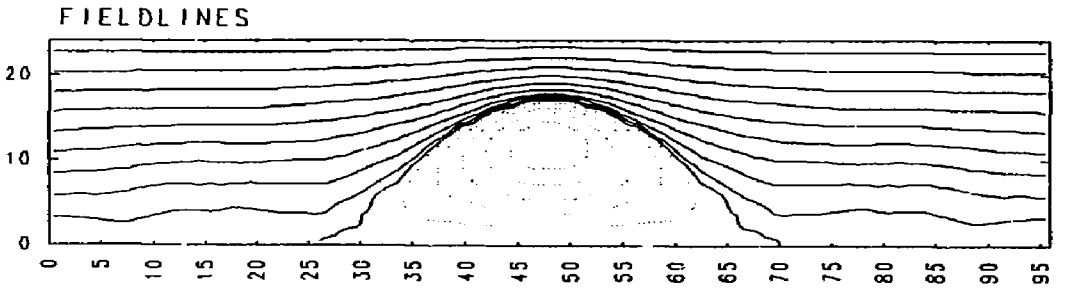
FIELDLINES
20
10
0
0 5 10 15 20 25 30 35 40 45 50 55 60 65 70 75 80 85 90 95

EXDA

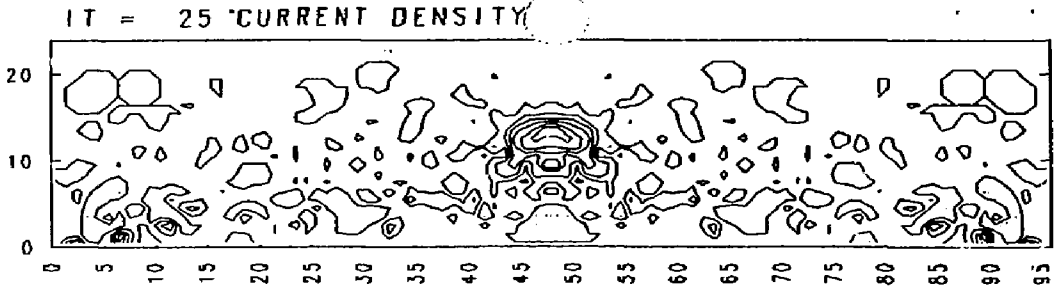
IT = 25 CURRENT DENSITY
20
10
0
0 5 10 15 20 25 30 35 40 45 50 55 60 65 70 75 80 85 90 95

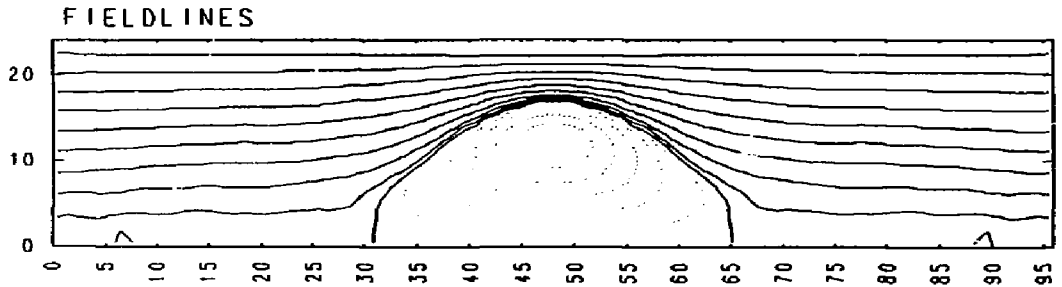
FIELDLINES
20
10
0
0 5 10 15 20 25 30 35 40 45 50 55 60 65 70 75 80 85 90 95

EXDA

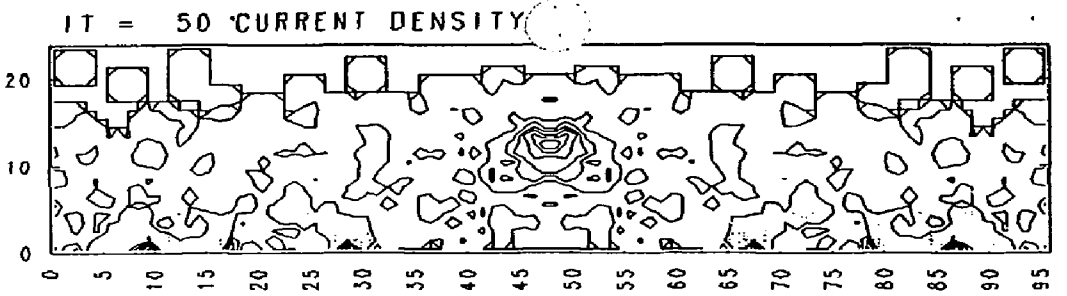
IT = 50 CURRENT DENSITY
20
10
0
0 5 10 15 20 25 30 35 40 45 50 55 60 65 70 75 80 85 90 95

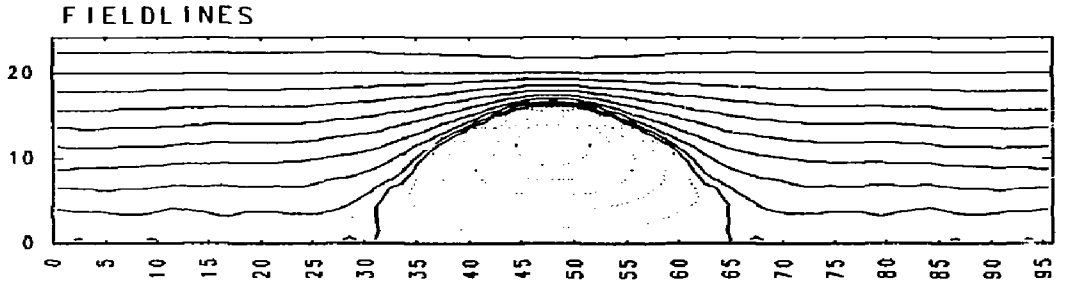
FIELDLINES
20
10
0
0 5 10 15 20 25 30 35 40 45 50 55 60 65 70 75 80 85 90 95

EXOA

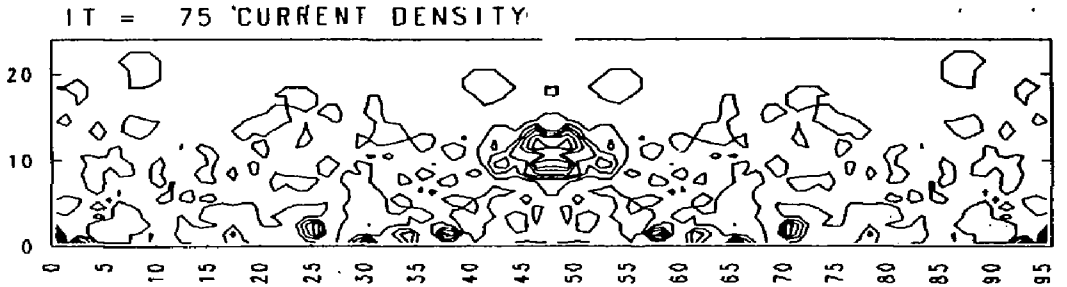
IT = 75 CURRENT DENSITY
20
10
0
0 5 10 15 20 25 30 35 40 45 50 55 60 65 70 75 80 85 90 95

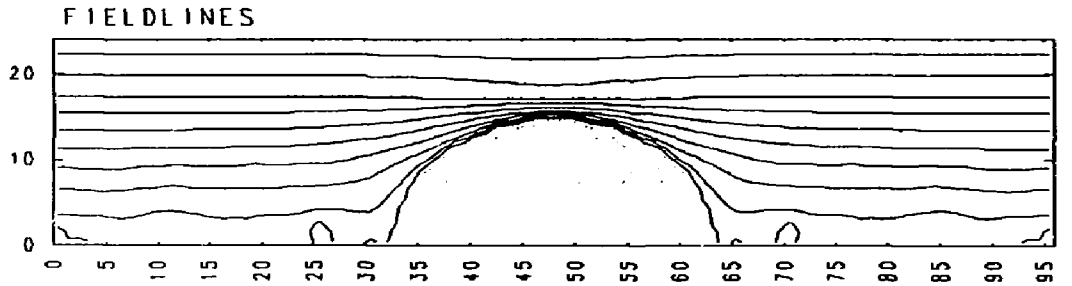
FIELDLINES
20
10
0
0 5 10 15 20 25 30 35 40 45 50 55 60 65 70 75 80 85 90 95

EXDA

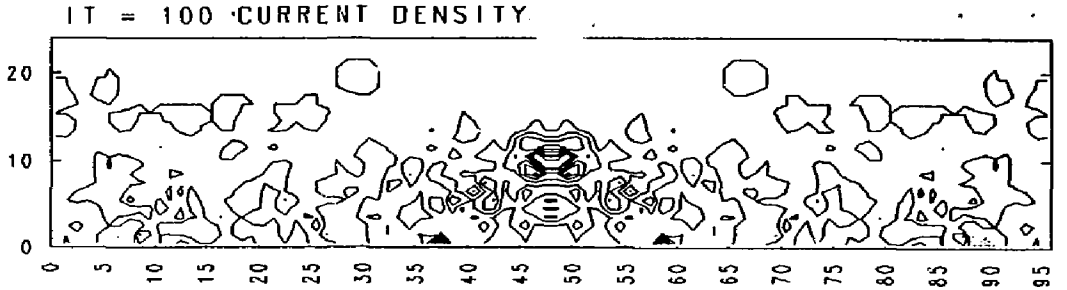
IT = 100 CURRENT DENSITY
20
10
0
0 5 10 15 20 25 30 35 40 45 50 55 60 65 70 75 80 85 90 95

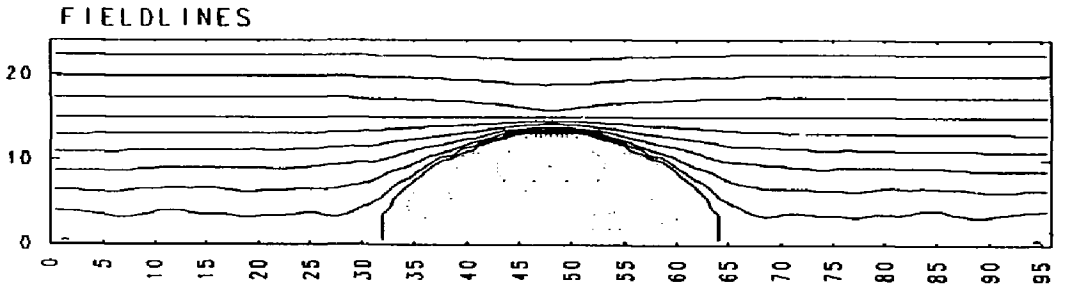
FIELDLINES
20
10
0
0 5 10 15 20 25 30 35 40 45 50 55 60 65 70 75 80 85 90 95

EXDA

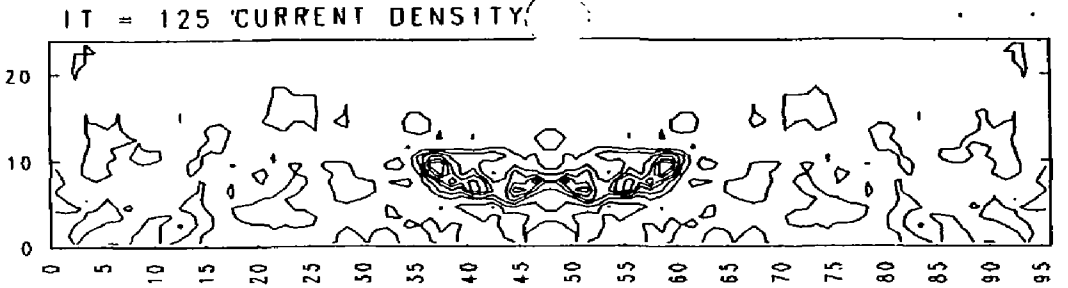
IT = 125 CURRENT DENSITY
20
10
0
0 5 10 15 20 25 30 35 40 45 50 55 60 65 70 75 80 85 90 95

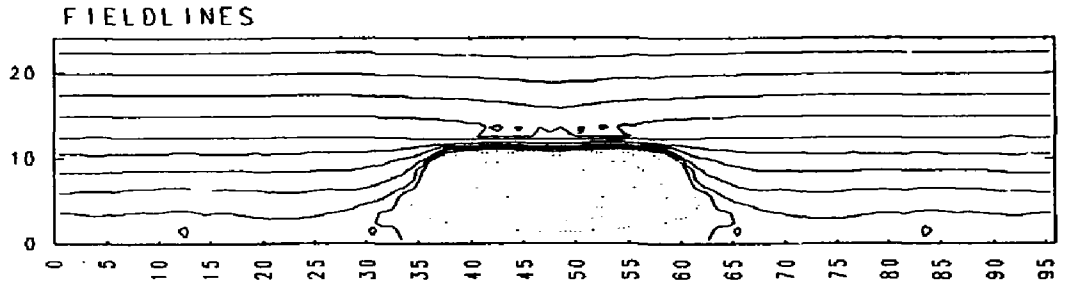
FIELDLINES
20
10
0
0 5 10 15 20 25 30 35 40 45 50 55 60 65 70 75 80 85 90 95

EXDA

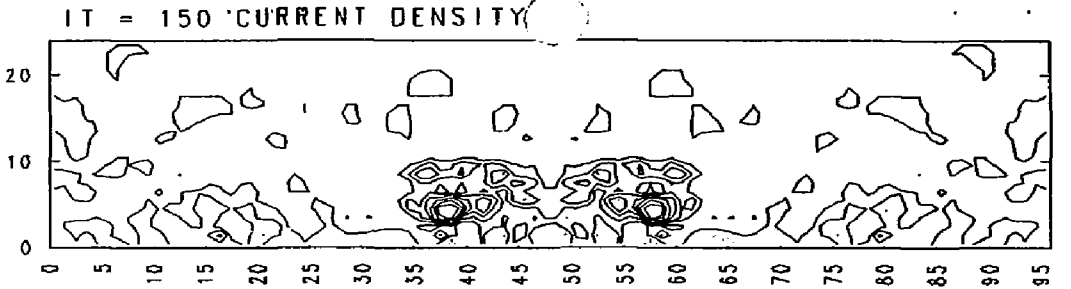
IT = 150 CURRENT DENSITY
20
10
0
0 5 10 15 20 25 30 35 40 45 50 55 60 65 70 75 80 85 90 95

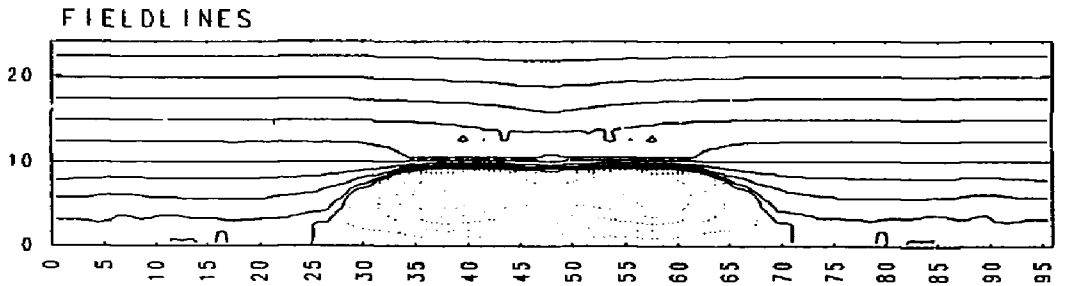
FIELDLINES
20
10
0
0 5 10 15 20 25 30 35 40 45 50 55 60 65 70 75 80 85 90 95

EXDA

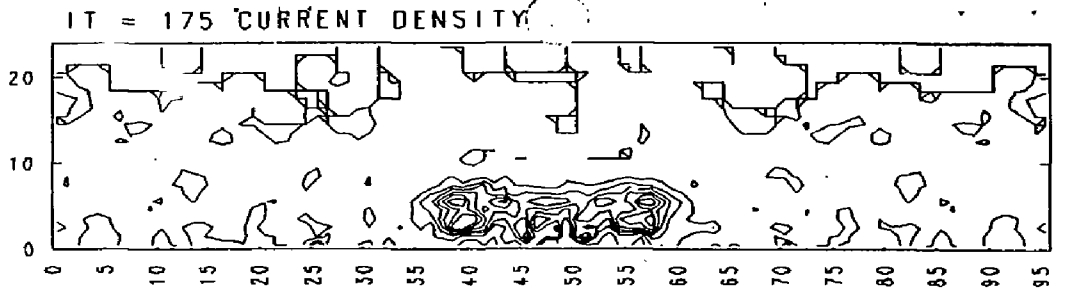
IT = 175 CURRENT DENSITY
20
10
0
0 5 10 15 20 25 30 35 40 45 50 55 60 65 70 75 80 85 90 95

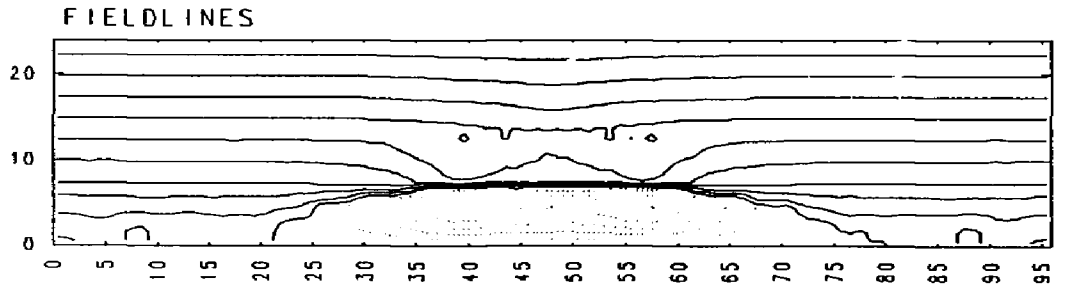
FIELDLINES
20
10
0
0 5 10 15 20 25 30 35 40 45 50 55 60 65 70 75 80 85 90 95

EXDA

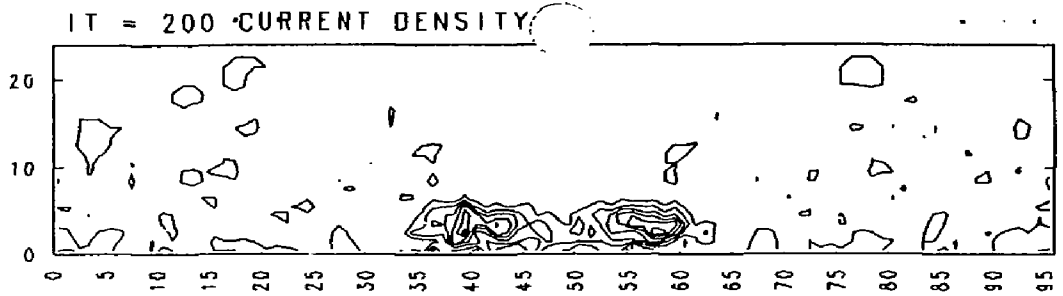
IT = 200 CURRENT DENSITY
20
10
0
0 5 10 15 20 25 30 35 40 45 50 55 60 65 70 75 80 85 90 95

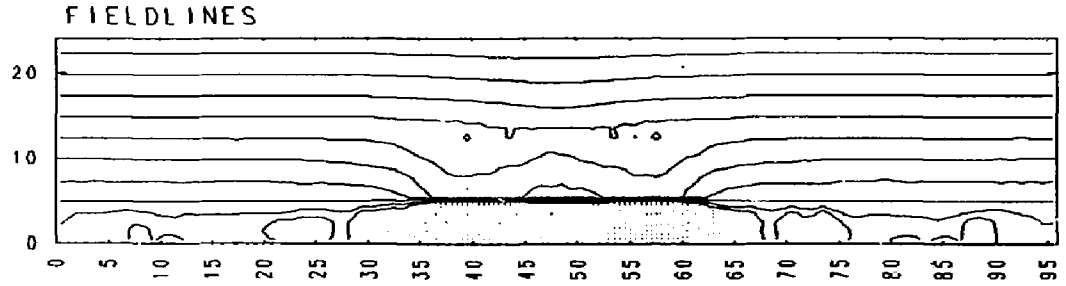
FIELDLINES
20
10
0
0 5 10 15 20 25 30 35 40 45 50 55 60 65 70 75 80 85 90 95

EXDA

BZX, BZMAX, BZAXIS

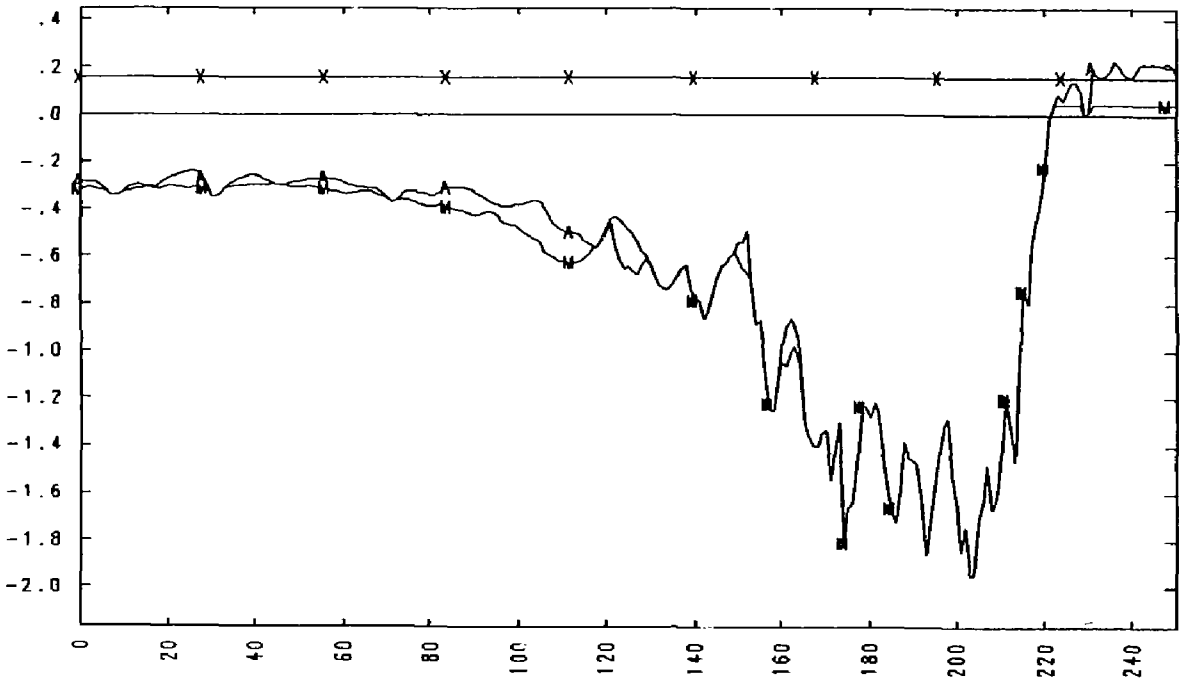

EXDA

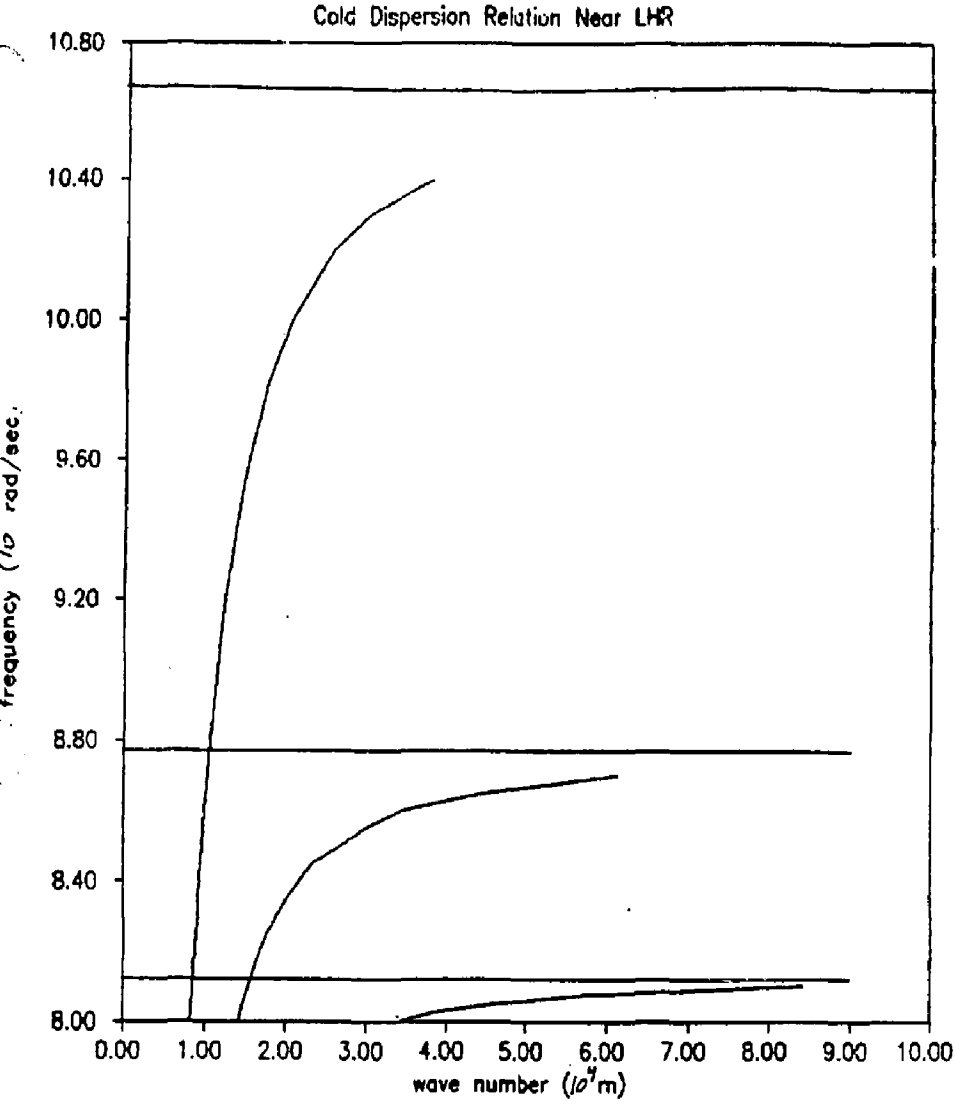
Cold Dispersion Relation Near LHR
10.80
10.40
10.00
9.60
9.20
8.80
8.40
8.00
frequency (10^9 rad/sec.)
0.00
1.00
2.00
3.00
4.00
5.00
6.00
7.00
8.00
9.00
10.00
wave number (10^4 m)

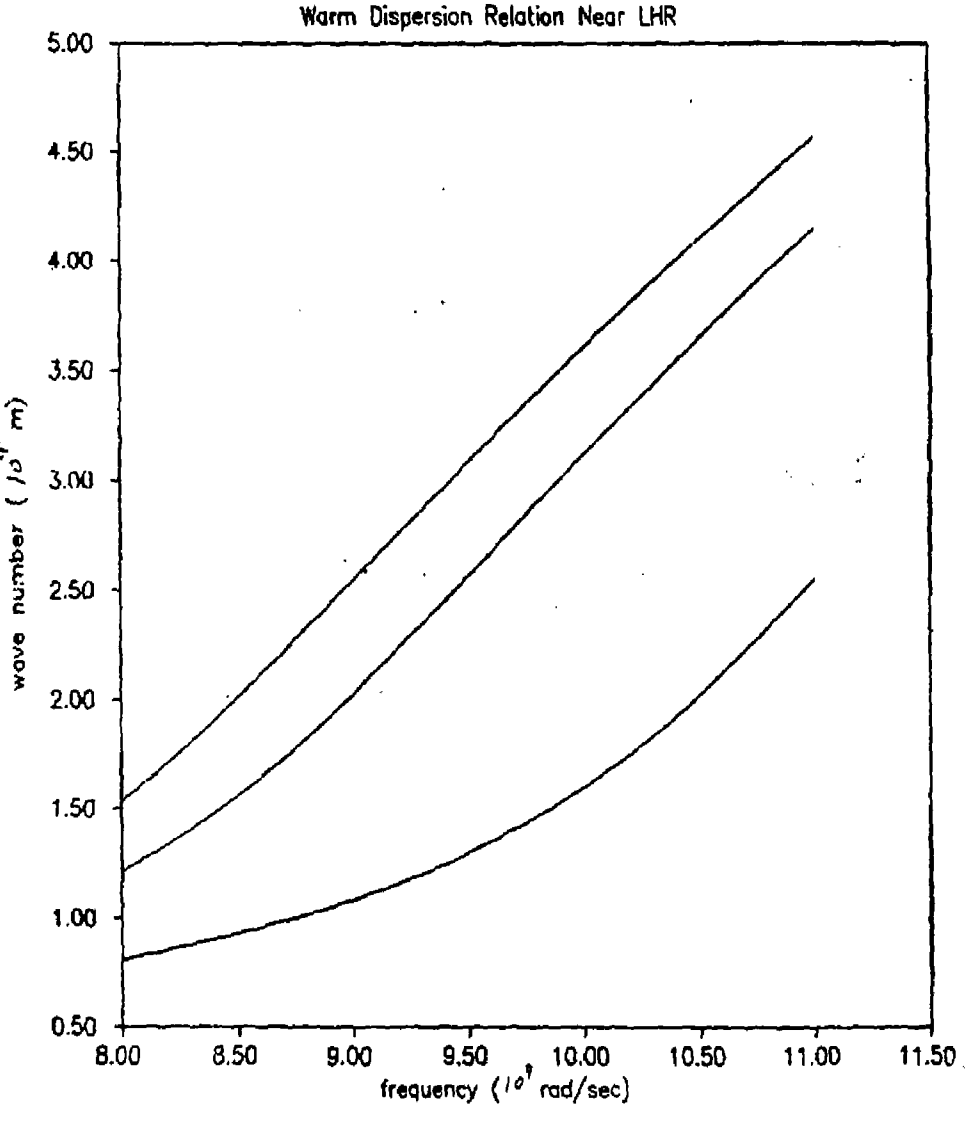
Warm Dispersion Relation Near LHR
5.00
4.50
4.00
3.50
3.00
2.50
2.00
1.50
1.00
0.50
wave number (10^{3} m)
8.00
8.50
9.00
9.50
10.00
10.50
11.00
11.50
frequency (10^{9} rad/sec)